Optics Letters

Nanophotonic tantala waveguides for supercontinuum generation pumped at 1560 nm

KIERAN F. LAMEE,[1,2] DAVID R. CARLSON,[1,2,*] ZACHARY L. NEWMAN,[1,2] SU-PENG YU,[1,2] AND SCOTT B. PAPP[1,2]

[1]*Time and Frequency Division, National Institute of Standards and Technology, 325 Broadway MS847, Boulder, Colorado 80305, USA*
[2]*Department of Physics, University of Colorado, 390 UCB, Boulder, Colorado 80309, USA*
Corresponding author: david.carlson@nist.gov

We experimentally demonstrate efficient and broadband supercontinuum generation in nonlinear tantala (Ta_2O_5) waveguides using a 1560 nm femtosecond seed laser. With incident pulse energies as low as 100 pJ, we create spectra spanning up to 1.6 octaves across the visible and infrared. Fabricated devices feature propagation losses as low as 10 dB/m, and they can be dispersion engineered through lithographic patterning for specific applications. We show a waveguide design suitable for low-power self-referencing of a fiber frequency comb that produces dispersive-wave radiation directly at the second-harmonic wavelength of the seed laser. A fiber-connectorized, hermetically sealed module with 2 dB per facet insertion loss and watt-level average-power handling is also described. Highly efficient and fully packaged tantala waveguides may open new possibilities for the integration of nonlinear nanophotonics into systems for precision timing, quantum science, biological imaging, and remote sensing. © 2020 Optical Society of America

https://doi.org/10.1364/OL.396950

Nonlinear waveguides based on integrated photonics can enable broadband and coherent supercontinuum generation (SCG) with picojoule pulse energies [1–4]. Leveraging nanoscale fabrication techniques, these waveguides can reduce the size, complexity, and power consumption associated with spectral broadening compared to traditionally used nonlinear fibers. Moreover, dispersion engineering via changes to the waveguide geometry can enable fine optimization of the output spectrum specific for individual applications [5–7]. While sub-micrometer dimensions are a key feature for nonlinear waveguides, they require the use of precision multi-axis positioning stages for alignment to standard free-space or fiber-coupled laser systems. A compact and sturdy packaging solution that does not compromise coupling efficiency is necessary for wide adoption of nonlinear SCG waveguides and for applications outside the laboratory.

Many different nonlinear photonic materials suitable for broadband SCG are available [8–14]. One particularly promising option is tantalum pentoxide (Ta_2O_5, henceforth, tantala)

[15]. Tantala is a commonly used and low-loss optical material in high-reflector dielectric Bragg mirrors [16] and has been demonstrated to support ultra-low waveguide propagation losses below 3 dB/m [17]. It is suited for applications in broadband nonlinear photonics due to its extremely broad transparency window spanning from the ultraviolet (300 nm) to the mid-infrared (8000 nm). Additionally, the nonlinear refractive index ($n_2 = 6.2 \times 10^{15}\,cm^2/W$) is three times higher than silicon nitride, and it has processing temperatures $< 550°C$ for back-end compatibility with other integrated-photonics platforms [18].

In this Letter, we use telecom-wavelength femtosecond seed pulses at 1550 nm to experimentally demonstrate dispersion-engineered SCG in tantala waveguides that span 1.6 octaves across the visible and near-infrared spectral regions. The waveguides exhibit low propagation and coupling losses and can have either an air-clad or fully oxide-clad geometry. We demonstrate a fully packaged SCG module designed for efficient f-to-$2f$ self-referencing of a fiber frequency comb. The module features an oxide-clad tantala waveguide, polarization-maintaining fiber leads, and hermetic sealing in a stainless-steel enclosure.

To fabricate the air-clad waveguide devices, we first deposit tantala to a thickness of 570 nm on a thermally oxidized silicon substrate via ion-beam sputtering. To reduce propagation losses, the films are then annealed overnight in a 25% O_2 environment at 550°C. The mask pattern is transferred to the tantala layer via electron-beam lithography (EBL) and a subsequent fluorine-based inductively coupled plasma (ICP) etch. After substrate cleaning, the wafer is diced into chips via deep reactive ion etching. To improve coupling to lensed fibers and free-space optics by increasing the mode size, the air-clad waveguides taper to a width of 3 µm at the facets.

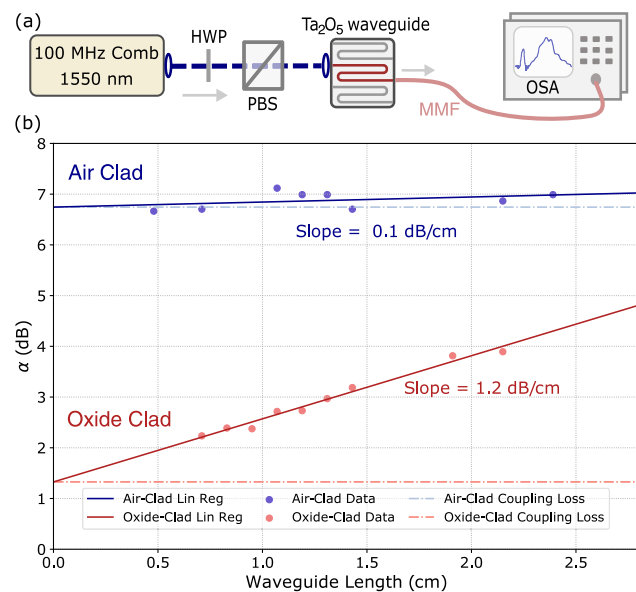Oxide-clad devices are made in a similar manner, and they have a tantala layer thickness of 800 nm for optimal dispersion engineering with telecom-C-band pump sources. Due to the high etch resistance of tantala and the additional layer thickness compared to the air-clad devices, we use a two-step etch, including a 180 nm titanium hard mask. We create a pattern for the titanium layer by way of EBL, and we transfer the pattern with Cl_2 plasma etching. The patterned substrate then undergoes a fluorine plasma etch to pattern the tantala layer. We strip the

wafer and remaining titanium before we deposit a top SiO$_2$ cladding layer via ICP chemical vapor deposition (ICP-CVD) to a thickness of 2 μm. Then, we perform rapid thermal annealing at 500°C for 1 h before dicing to reduce cladding absorption losses. The oxide-clad devices have inverse tapers at each facet with a length of 200 μm and a minimum width of 200 nm for efficient edge coupling.

The experimental schematic for characterizing our tantala SCG waveguides is shown in Fig. 1(a). We use a mode-locked all-polarization-maintaining fiber laser, producing 80 fs pulses with a center wavelength of 1560 nm, an average power of 100 mW, and a repetition rate of 100 MHz as the seed for SCG [19]. We collimate the laser output in free space; the beam passes through a half-wave plate and polarizing beam splitter pair for linear attenuation of the pulses incident on the waveguides. An aspheric lens with a numerical aperture of 0.6 is used for the input coupling to the fundamental quasi-transverse-electric mode of the waveguide. For loss measurements, a second identical aspheric lens is used to collimate the waveguide output to measure out-coupled power. However, for SCG spectrum measurements, a butt-coupled fluoride multi-mode fiber collects the waveguide output and delivers it to an optical spectrum analyzer.

We characterize the per-facet coupling loss (α_{facet}) and propagation loss (α_{prop}) by fabricating a chip containing multiple waveguides of varying lengths L, but with identical widths ($w = 1.4$ μm) and edge couplers. We wrap the waveguides in a meandering pattern [see Fig. 1(a)] with a radius of 100 μm to minimize bend-induced losses. We measure the ratio of incident laser power P_{in} to out-coupled power P_{out} in free space for each length of waveguide and calculate the losses by fitting a line of the form $\alpha = -10 \log(P_{\text{in}}/P_{\text{out}}) = 2\alpha_{\text{facet}} + L\alpha_{\text{prop}}$.

Figure 1(b) shows the measured total loss (α) for both air-clad and oxide-clad waveguides as a function of length. We assume

the coupling losses are consistent for a few chips produced at the same time from one wafer; hence, the data all have the same y-intercept point. We estimate $\alpha_{\text{facet}} = 3.4$ dB for air-clad devices and $\alpha_{\text{facet}} = 0.7$ dB for oxide-clad devices, which have inverse tapers for mode matching. The fitted slope yields a propagation loss at 1560 nm of $\alpha_{\text{prop}} = 0.1$ dB/cm for the air-clad waveguides and $\alpha_{\text{prop}} = 1.2$ dB/cm for devices with a top oxide cladding. We attribute the additional absorption losses in the oxide cladding to a combination of residual contamination from the titanium mask and to hydrogen impurities originating from the SiH$_4$ precursor gas used in the ICP-CVD deposition [20]. The SiO$_2$ top-cladding loss could likely be reduced to negligible levels by instead using a tetraethyl orthosilicate (TEOS)-based precursor [21] or by directly sputter depositing the oxide film onto the patterned tantala wafer [17].

Like other material platforms available for high-confinement nonlinear waveguides, tantala supports broad group-velocity dispersion (simply *dispersion* below) engineering capabilities through control of the geometric dispersion. Figure 2 shows how the supercontinuum power-spectral density (PSD) in air-clad 570 nm thick devices can be tuned by changing the waveguide width alone. For example, the short-wavelength dispersive wave can be tuned from ∼640 nm at a waveguide width of 1.2 μm to ∼900 nm for a width of 1.7 μm. The input pulse energy (0.9 nJ) in each case is well beyond the threshold for soliton fission and is chosen to accentuate the dispersive-wave shifts. In each case, the plotted spectra are stitched together using a grating spectrometer for wavelengths <1750 nm and a Fourier-transform spectrometer for wavelengths >1750 nm. The plotted PSD is scaled to intra-waveguide levels by adding a constant offset of +6.7 dB, to account for broadband coupling losses to the butt-coupled multi-mode collection fiber.

The calculated dispersion for each waveguide in Fig. 2 is shown in (a) and is obtained from a finite-difference mode
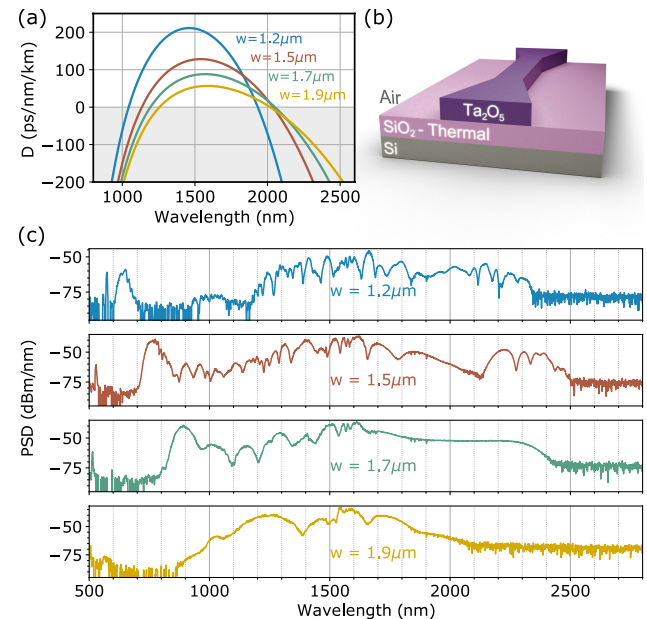

Fig. 1. Tantala waveguide characterization. (a) Experimental schematic for SCG measurements. PBS, polarizing beam splitter; HWP, half-wave plate; MMF, multi-mode fiber; OSA, optical spectrum analyzer. (b) Measured waveguide propagation loss for air-clad (blue) and oxide-clad (red) devices. Dashed lines indicate the extracted total facet-coupling losses.

Fig. 2. (a) Calculated waveguide dispersion for 570 nm thick air-clad devices of varying widths w. (b) Material cross section (not to scale) for the air-clad tantala waveguides. (c) Experimental supercontinuum PSD from four different waveguide widths at 80 fs pulse duration and 0.9 nJ/pulse.
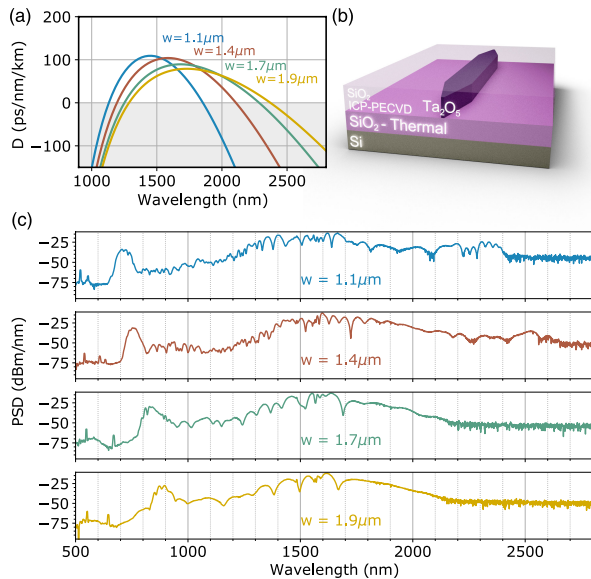
Fig. 3.   (a) Calculated waveguide dispersion for 800 nm thick oxide-clad devices of varying widths w. (b) Material cross section (not to scale) for the oxide-clad tantala waveguides. (c) Experimental supercontinuum PSD from four different waveguide widths at 80 fs pulse duration and 0.9 nJ/pulse.
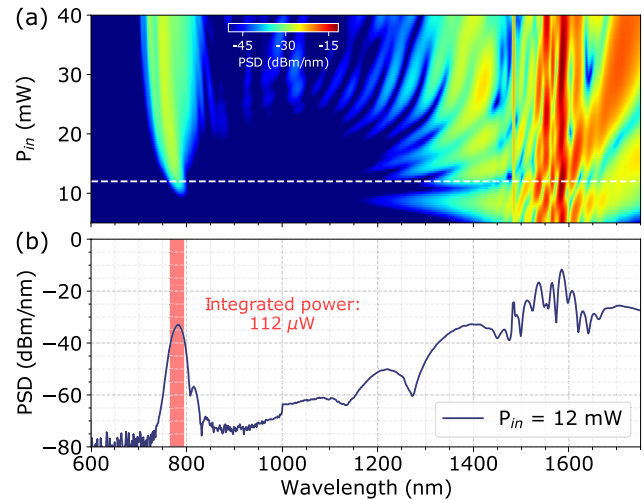

Fig. 4.   (a) Experimental output spectrum of an oxide-clad waveguide designed for f-to-$2f$ stabilization as a function of incident laser power. (b) Line-out spectrum at 12.0 mW incident power [dashed white line in (a)]. Waveguide parameters: $w = 1.45$ µm, $L = 5$ mm, 800 nm thickness.

solver [22], using refractive index data for SiO_2 from [23] and tantala index data measured via ellipsometry. A more precise understanding of the tantala dispersion and its role in nonlinear processes, such as SCG, is a goal of future work.

The SCG spectral measurements and dispersion calculations, repeated for the 800 nm thick oxide-clad waveguides, are shown in Fig. 3. The dispersion profiles for waveguides of width > 1.5 µm suggest that the long-wavelength dispersive wave in these devices should extend out to a wavelength of 3000 nm. However, this is not observed experimentally, likely due to absorption losses in the oxide cladding [11]. To take advantage of the full mid-infrared transparency window of tantala, a suspended-ridge geometry could be explored [24].

Low-power f-to-$2f$ self-referencing of an optical frequency comb is one application that can benefit from the dispersion engineering offered by nanophotonic waveguides [3]. By generating a 780 nm dispersive wave at the second-harmonic wavelength of the pump laser directly from the waveguide, the frequency-doubling component of f-to-$2f$ detection can be completely decoupled from the SCG. This simplifies the f-to-$2f$ detection process in comparison to techniques that double light from the long-wavelength portion of the SCG spectrum.

In the oxide-clad waveguides, a 780 nm harmonic dispersive wave corresponds to a waveguide width of 1.45 µm. The waveguide output, collected by a lensed fiber, is shown in Fig. 4(a) as a function of incident laser power by attenuating the beam with the free-space half-wave plate and polarizer. The plotted PSD has a $+ 3.7$ dB offset to account for additional coupling losses in the output lensed fiber and is representative of the intra-waveguide power levels. Figure 4(b) shows a line-out spectrum at an incident laser power of 12.0 mW.

Efficient and durable fiber-to-chip coupling interfaces [25–27] are needed for nonlinear integrated photonics devices to be used outside of the laboratory. However, SCG waveguides still

pose critical challenges for photonics packaging since both high peak and average optical powers must be supported, while also efficiently coupling large (> 10 THz) optical bandwidths.

The packaged tantala waveguide shown in Fig. 5(a) is designed to produce a 780 nm dispersive wave for f-to-$2f$ self-referencing of a low-power 1560 nm fiber frequency comb. The waveguide itself is fully oxide clad, has a length of 13.4 mm, a width of 1.45 µm, and a thickness of 800 nm. The stainless-steel enclosure is hermetically sealed and has a total volume < 12 cm^3. The input and output fibers (PM1550 and PM780, respectively) are polarization maintaining, and we splice them to 1.5 mm segments of ultra-high numerical-aperture fiber (NA = 0.35) for mode matching to the waveguide's inverse-taper edge couplers. Each fiber butt-couples to the waveguide facet, and we hand-apply a small drop of low-shrinkage UV-curable adhesive to each side of the fiber. Because the fiber is pressed tightly against the chip, no realignment is necessary after applying the glue. This approach avoids any adhesive interacting with the optical mode but still maintains a direct bond between the fiber and chip.

After curing, the PM1550 input fiber has a fiber-to-chip insertion loss of 2 dB. When pumped at 1560 nm with a 200 pJ 230 fs pulse, the single-mode PM780 output fiber collects the spectrum shown in Fig. 5(c). The 780 nm dispersive-wave output exhibits good power stability during extended operation [power over 23 h period shown in Fig. 5(b)] for reliable comb stabilization. Figure 5(d) shows the detected offset frequency after optically heterodyning the output of a similar tantala module and 780 nm light generated via second-harmonic generation of the seed comb in a separate doubling crystal [3].

The package design is capable of withstanding > 10 kW peak powers and > 1 W average powers with no loss in coupling performance, though the ultimate performance limits have not yet been characterized. This wide operating range of optical powers is an important consideration for scaling SCG to higher repetition rates where higher average powers are necessary to deliver an equivalent pulse energy to the waveguide [28].
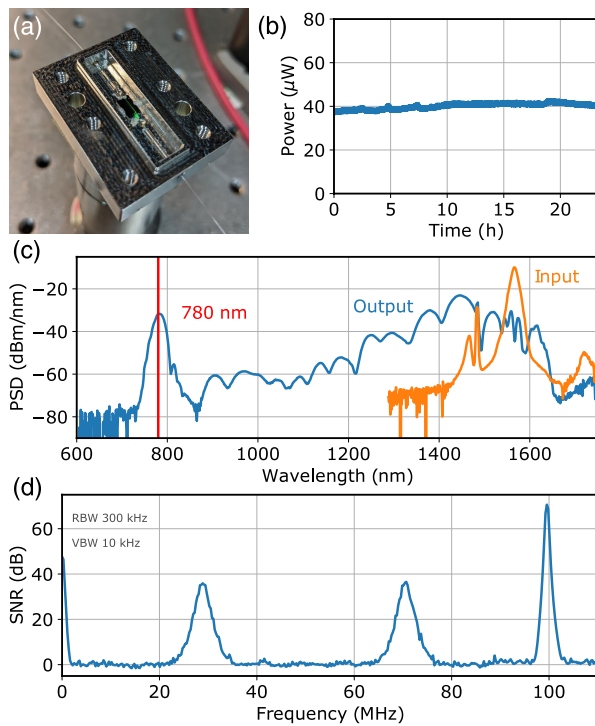
Fig. 5. (a) Photo of packaged supercontinuum module with lid removed. (b) Power stability of the module's fiber-coupled 780 nm dispersive wave over 23 h. (c) Output spectrum in PM780 fiber when pumped at 1560 nm with 230 fs pulses. The pulse energy in the PM1550 input fiber is 200 pJ. (d) Offset frequency of a 100 MHz repetition-rate comb detected at 780 nm after broadening in a packaged tantala waveguide. SNR, signal-to-noise ratio.

Our results suggest that tantala-based nonlinear waveguides can reduce the power requirements for ultrabroadband nonlinear optical processes at visible and infrared wavelengths. Further reductions in pulse energy compared to the present results are expected by fabricating longer waveguides and/or using shorter pump wavelengths [2,15]. The platform may also support all-in-one comb stabilization via f–$3f$ self-referencing [3], eliminating the need for external frequency doubling in comb applications. The combination of robust packaging along with low coupling and propagation losses will support demanding applications outside of the laboratory in the academic, commercial, and defense sectors.

REFERENCES

1. N. Nader, A. Kowligy, J. Chiles, E. J. Stanton, H. Timmers, A. J. Lind, F. C. Cruz, D. M. B. Lesko, K. A. Briggman, S. W. Nam, S. A. Diddams, and R. P. Mirin, Optica **6**, 1269 (2019).

2. A. Klenner, A. S. Mayer, A. R. Johnson, K. Luke, M. R. E. Lamont, Y. Okawachi, M. Lipson, A. L. Gaeta, and U. Keller, Opt. Express **24**, 11043 (2016).

3. D. R. Carlson, D. D. Hickstein, A. Lind, S. Droste, D. Westly, N. Nader, I. Coddington, N. R. Newbury, K. Srinivasan, S. A. Diddams, and S. B. Papp, Opt. Lett. **42**, 2314 (2017).

4. N. Singh, M. Xin, D. Vermeulen, K. Shtyrkova, N. Li, P. T. Callahan, E. S. Magden, A. Ruocco, N. Fahrenkopf, C. Baiocco, B. P.-P. Kuo, S. Radic, E. Ippen, F. X. Kärtner, and M. R. Watts, Light Sci. Appl. **7**, 17131 (2018).

5. H. Liang, Y. He, R. Luo, and Q. Lin, Opt. Express **24**, 29444 (2016).

6. D. R. Carlson, D. D. Hickstein, A. Lind, J. B. Olson, R. W. Fox, R. C. Brown, A. D. Ludlow, Q. Li, D. Westly, H. Leopardi, T. M. Fortier, K. Srinivasan, S. A. Diddams, and S. B. Papp, Phys. Rev. Appl. **8**, 014027 (2017).

7. Y. Okawachi, M. Yu, J. Cardenas, X. Ji, M. Lipson, and A. L. Gaeta, Opt. Lett. **42**, 4466 (2017).

8. D. Y. Oh, K. Y. Yang, C. Fredrick, G. Ycas, S. A. Diddams, and K. J. Vahala, Nat. Commun. **8**, 13922 (2017).

9. B. Kuyken, T. Ideguchi, S. Holzner, M. Yan, T. W. Hänsch, J. Van Campenhout, P. Verheyen, S. Coen, F. Leo, R. Baets, G. Roelkens, and N. Picqué, Nat. Commun. **6**, 6310 (2015).

10. M. Jankowski, C. Langrock, B. Desiatov, A. Marandi, C. Wang, M. Zhang, C. R. Phillips, M. Lončar, and M. M. Fejer, "Ultrabroadband nonlinear optics in nanophotonic periodically poled lithium niobate waveguides," arXiv:1909.08806 [physics] (2019).

11. D. D. Hickstein, H. Jung, D. R. Carlson, A. Lind, I. Coddington, K. Srinivasan, G. G. Ycas, D. C. Cole, A. Kowligy, C. Fredrick, S. Droste, E. S. Lamb, N. R. Newbury, H. X. Tang, S. A. Diddams, and S. B. Papp, Phys. Rev. Appl. **8**, 014025 (2017).

12. J. P. Epping, T. Hellwig, M. Hoekman, R. Mateman, A. Leinse, R. G. Heideman, A. van Rees, P. J. van der Slot, C. J. Lee, C. Fallnich, and K.-J. Boller, Opt. Express **23**, 19596 (2015).

13. B. Kuyken, M. Billet, F. Leo, K. Yvind, and M. Pu, Opt. Lett. **45**, 603 (2020).

14. Y. Yu, X. Gai, T. Wang, P. Ma, R. Wang, Z. Yang, D.-Y. Choi, S. Madden, and B. Luther-Davies, Opt. Mater. Express **3**, 1075 (2013).

15. R. Fan, C.-L. Wu, Y.-Y. Lin, C.-Y. Liu, P.-S. Hwang, C.-W. Liu, J. Qiao, M.-H. Shih, Y.-J. Hung, Y.-J. Chiu, A.-K. Chu, and C.-K. Lee, Opt. Lett. **44**, 1512 (2019).

16. S. Reid and I. Martin, Coatings **6**, 61 (2016).

17. M. Belt, M. L. Davenport, J. E. Bowers, and D. J. Blumenthal, Optica **4**, 532 (2017).

18. H. Jung, S.-P. Yu, D. R. Carlson, T. E. Drake, T. C. Briles, and S. B. Papp, in *Nonlinear Optics (NLO)*, OSA (Hawaii, USA, 2019), paper NW2A.3.

19. L. C. Sinclair, J.-D. Deschênes, L. Sonderhouse, W. C. Swann, I. H. Khader, E. Baumann, N. R. Newbury, and I. Coddington, Rev. Sci. Instrum. **86**, 081301 (2015).

20. F. Ay and A. Aydinli, Opt. Mater. **26**, 33 (2004).

21. T. A. Huffman, G. M. Brodnik, C. Pinho, S. Gundavarapu, D. Baney, and D. J. Blumenthal, IEEE J. Sel. Top. Quantum Electron. **24**, 5900209 (2018).

22. A. B. Fallahkhair, K. S. Li, and T. E. Murphy, J. Lightwave Technol. **26**, 1423 (2008).

23. I. H. Malitson, J. Opt. Soc. Am. **55**, 1205 (1965).

24. M. Vlk, V. Mittal, G. S. Murugan, and J. Jagerska, Conference on Lasers and Electro-Optics Europe & European Quantum Electronics Conference (CLEO/Europe-EQEC), Munich, Germany (IEEE, 2019), pp. 1.

25. A. S. Raja, J. Liu, N. Volet, R. N. Wang, J. He, E. Lucas, R. Bouchandand, P. Morton, J. Bowers, and T. J. Kippenberg, Opt. Express **28**, 2714 (2020).

26. T. G. Tiecke, K. P. Nayak, J. D. Thompson, T. Peyronel, N. P. D. Leon, V. Vuletić, and M. D. Lukin, Optica **2**, 70 (2015).

27. J. Nauriyal, M. Song, R. Yu, and J. Cardenas, Optica **6**, 549 (2019).

28. D. R. Carlson, D. D. Hickstein, W. Zhang, A. J. Metcalf, F. Quinlan, S. A. Diddams, and S. B. Papp, Science **361**, 1358 (2018).